THE AMERICAN SOCIETY OF MECHANICAL ENGINEERS
345 E. 47th St., New York, N.Y. 10017

97-GT-297

A CFD BENCHMARK STUDY:

LEADING EDGE FILM-COOLING WITH COMPOUND ANGLE INJECTION

C. A. Martin and K. A. Thole
Mechanical Engineering Department
University of Wiscsonsin
Madison, Wisconsin 53706

ABSTRACT

This paper presents a blind CFD benchmark of a simulated leading edge for a turbine airfoil. The geometry studied was relevant for current designs with two rows of staggered film-cooling holes located at the stagnation location ($\theta = 0°$) and at $\theta = 25°$. Both rows of cooling holes were blowing in the same direction which was 90° relative to the streamwise direction and had an injection angle with respect to the surface of 20°. Realistic engine conditions were simulated including a density ratio of DR = 1.8 and an average blowing ratio of M = 2 for both rows of cooling holes. This blind benchmark coincided with an experimental study that took place in a wind tunnel simulation of a quarter cylinder followed by a flat afterbody. At the stagnation region, the CFD calculation overpredicted the adiabatic effectiveness because the model failed to predict a small separation region that was measured in the experiments. Good agreement was achieved, however, between the CFD predictions and the experimentally measured values of the laterally averaged adiabatic effectiveness downstream of the stagnation location. The coolant pathlines showed that flow passed from the first row of holes over the second row of cooling holes indicating a waste of the coolant.

INTRODUCTION

To provide high efficiency turbine engines, modern day components operate in environments with temperatures much higher than the maximum permissible blade alloy temperatures. The desire to further improve efficiencies by increasing exiting combustor temperatures requires cooling critical edges of the downstream blades. In particular, the leading edge of an airfoil is subjected to very high temperatures with high levels of freestream turbulence. Cooling this region is commonly accomplished by convective cooling and film-cooling. Convective cooling takes place both inside the airfoil and through film-cooling passages that are strategically placed in the vane surface. Film-cooling is achieved after the convective fluid exits these cooling passages to protect the outside surface. Film-cooling the leading edge is particularly critical to protect the stagnation region of the airfoil. Both the average airfoil temperatures as well as the local surface temperature variance need to be considered to achieve a workable film-cooling design. Additionally, cooling needs to be accomplished with a minimal amount of fluid since this working fluid loss can reduce the engine's thermodynamic performance.

To efficiently cool the leading edge of an airfoil, there is an overwhelming number of different geometrical and flow parameters to be considered. For example, the cooling hole injection angle, row and hole spacing and placement relative to the stagnation point, and hole shape are all geometrical parameters that ultimately affect the amount of coolant required to efficiently cool the leading edge. Some of the flow parameters that can influence the surface heat transfer include jet-to-mainstream momentum flux ratios, Reynolds number, and freestream turbulence levels. To provide a complete understanding of all of these parameters through experimentation requires an extensive test matrix. If, however, there was a reliable predictive tool that could be used to guide the experiments, the design process could be made more efficient.

This paper focuses on benchmarking a Reynolds-averaged, Navier-Stokes (RANS) code to predict film-cooling adiabatic effectiveness for a cylindrical leading edge with a flat afterbody. This flowfield is very complex in that there are high acceleration and curvature effects in addition to the complicated film-cooling jet itself. This CFD benchmark was completed simultaneously with an on-going experimental study by Cruse, Yuki, and Bogard (1997). The results presented in this paper represent a blind benchmark in that the data was not known until after the computational results were submitted to the sponsors. Prior to simulating the leading edge film-cooling geometry, an in-house study was done for a film-cooling flow over a flat plate to benchmark the code with data that was already available in the open literature. This paper will present both benchmarks with only the leading edge simulation being the blind benchmark.

After a brief discussion of relevant past leading edge film-cooling studies, the remainder of this document presents the computational methodology used for the studies presented in this paper, a brief discussion regarding the flat plate film-cooling benchmark, results for the leading edge benchmark, and finally some conclusions. In the leading edge benchmark, comparisons will be discussed between the CFD results and the experimental results presented by Cruse, et al. (1997).

Presented at the International Gas Turbine & Aeroengine Congress & Exhibition
Orlando, Florida — June 2–June 5, 1997

PAST STUDIES

The only detailed CFD studies for the leading edge region of an airfoil were those presented by Benz, et al. (1993), Zhou, et al. (1993) and He, et al. (1996). Benz, et al. (1993) performed a two-dimensional simulation with slot film-cooling on an actual turbine vane geometry and found that the coolant flow inside the hole is affected by the main flow at the hole exit. Zhou, et al. (1993) completed a number of CFD studies in which they simulated their own experimental data base (Salcudean, et al., 1994) that used a scaled-up cylinder having two rows of film-cooling holes located at ±15° and ±44°. They showed good agreement at the low blowing ratio of M = 0.5. However, when their jet separated at M = 1.2, their CFD results overpredicted their adiabatic effectiveness measurements.

The majority of the leading edge studies presented in the open literature have been experimental simulations. Using a circular cylinder in a crossflow and the napthalene sublimation technique, Karni and Goldstein (1990) determined how film-cooling coverage is affected when the location of the jet injection is moved relative to the stagnation point. They showed that the mass transfer coefficients were highly skewed when the injection location moved just 3° off the stagnation point. Karni and Goldstein also pointed out the importance of quantifying the heat transfer coefficients since they showed that mass transfer coefficients (analogous to convective heat transfer coefficients) could be two and three times higher as a result of film-cooling the cylinder in comparison to no film-cooling on the cylinder.

Mick and Mayle (1988) and Mayle and Anderson (1991) presented detailed adiabatic effectiveness, convective heat transfer coefficients, and flow and thermal field profiles near a stagnation region of a circular leading edge. They used three rows of staggered, spanwise-directed, cooling holes located at ±15° and +44°. These locations provided different static pressures and as a result a large disparity in the exiting mass flowrates for the two rows of holes. Although average blowing ratios of M = 0.38, 0.64, and 0.97 were investigated the M = 0.38 case resulted in a blowing ratio of $M_{15°} = 0.19$ for the 15° row and a blowing ratio of $M_{44°} = 0.57$ for the 44° row. Mick and Mayle (1988) also confirmed the importance of measuring the convective heat transfer coefficients for the film-cooled case which showed values as much as two to three times the un-cooled case and that the peak adiabatic effectiveness did not correspond to the peak convective heat transfer coefficient. The optimal blowing ratios for this geometry, in terms of overall reduced heat loads, was M = 0.64. The highest blowing ratio, M = 0.97, actually caused an increase in the amount of heat transfer which could primarily be attributed to the low adiabatic effectiveness values for these high momentum jets ($I_{15°} = 0.53$ and $I_{44°} = 1.56$).

A significant number of experimental leading edge film-cooling studies were done by Mehendale and Han (1992a, b), Mehendale and Han (1993), Ou, et al., (1992), Ou and Han (1992), and Ou and Han (1994) in which a number of different geometrical and flow effects were investigated. In general, these studies were done with a semi-circular blunt body followed by a flat afterbody that had staggered film-cooling holes (or slots in the case of Ou and Han, 1992 and 1994) located at ±15° and ±40°. Mehendale and Han's (1992a) results showed that in general film effectiveness decreases and the heat transfer coefficients increase with increasing freestream turbulence. Mehendale and Han (1992a) found that the optimal blowing ratio was M = 0.8 between the first and second row of holes and M = 0.4 after the second row of holes, which remained the same with or without high freestream turbulence. In contrast, Ou and Han (1992) showed that when using rows of slots, the optimal blowing ratio at low freestream turbulence was M = 0.4 and at high freestream turbulence was M = 0.8.

None of the geometries presented above, except for that of Karni and Goldstein (1990), have considered a cooling hole directly at the stagnation point with a very shallow spanwise injection angle, as in the case of this particular study which uses β = 20°. To date, the only CFD studies which have presented detailed adiabatic effectiveness predictions are those of He, et al. (1996) and Salcudean, et al. (1994). In addition, this particular study presents a "blind" CFD test case such that CFD is truly being tested for use as a design tool.

COMPUTATIONAL METHODOLOGY

To obtain accurate predictions of film-cooling flows, computational modeling must pay close attention to four major issues as outlined by Walters and Leylek (1996). These issues are the accuracy of geometry definition and quality of grid generation, the application of physically sound boundary conditions, the use of high-order discretization schemes,

Nomenclature

d	Film-cooling hole diameter
D	Leading edge diameter
DR	Jet-to-mainstream density ratio
h_o	Heat transfer coefficient without film-cooling, $q''/(T_w-T_\infty)$
h_f	Heat transfer coefficient with film-cooling, $q''/(T_{aw}-T_w)$
I	Jet-to-mainstream momentum flux ratio, $I = \rho_c U_c^2 / \rho_\infty U_\infty^2$
L	Cooling hole length
M	Jet-to-mainstream mass flux ratio, $M = \rho_c U_c / \rho_\infty U_\infty$
$P_{o,c}$	Stagnation pressure at hole entrance
p_∞	Upstream static pressure
r	Radial position inside the cooling hole
R_o	Outside radius of the cooling hole
Re_m	Reynolds number based on momentum thickness
S	Hole spacing
Tu	Turbulence level (%), see equation(1a)
TKE	Turbulent kinetic energy
U, V	Streamwise and vertical mean velocity components
U_c	Average coolant velocity from both rows of holes
u_τ	Friction velocity, $u_\tau = (\tau_w/\rho)^{0.5}$
VR	Jet-to-mainstream velocity ratio
x	Streamwise distance measured along the surface
x_h	Streamwise distance in the cooling hole from hole start
y	Vertical distance measured normal to the surface
y^+	Normalized vertical distance in wall coordinates, $y\, u_\tau / \nu$
z	Spanwise distance
Greek	
α	Angle of injection with respect to the mainstream
β	Angle of injection with respect to the surface
ε	Turbulence dissipation, equation (1b)
η	Adiabatic effectiveness, $(T_{aw} - T_\infty)/(T_c - T_\infty)$
ρ	Fluid density
θ	Angular position measured from stagnation
Θ	Non-dimensional fluid temperature, $(T - T_\infty)/(T_c - T_\infty)$
Subscripts and Superscripts	
—	Laterally averaged value
aw	Adiabatic wall
c	Coolant flow
w	Test plate surface
∞	Upstream conditions
o	No injection case

and the closure scheme for turbulence and near-wall modeling. The film-cooling studies presented in this paper paid close attention to each of these issues and, most importantly, the performance of two common turbulence models, which are the standard k-ε and RNG k-ε, and two near-wall treatments, which are the equilibrium and non-equilibrium wall functions. The CFD package used in these studies is a commercial package offered by Fluent, Inc. and is similar to the RAMPANT package used for simulating film-cooling flowfields by Walters and Leylek (1996). The particular package that was used for this study contains a pre-processor (Geomesh), an interior mesh generator (Tgrid), and an unstructured solution-adaptive incompressible flow solver (FLUENT/UNS).

The geometry and unstructured tetrahedral mesh in this study was generated with Geomesh and Tgrid. For both benchmark cases, a triangular surface mesh was created with Geomesh and the resulting three-dimensional tetrahedral meshes were created in Tgrid. The boundary mesh achieves an accurate representation of the geometry since it is mapped to mathematical surfaces defined in the geometry generation. Not only is the geometric accuracy of the boundary mesh important, but also the quality of the boundary mesh (i.e., cell skewness, grid stretching) because the three-dimensional grid is inherently dependent on it. Cell skewness is a measure of how the faces of adjacent cells are lined up. For a volume element, the average skewness is calculated by taking all pairs of adjacent faces and computing their normals and comparing those normals with those present in the volume. The scheme uses 0 to represent an equilateral volume and 1 to represent a deformed volume. Tgrid uses a Delauney Triangulation method and offers skewness-based smoothing and face-swapping, as well as user defined local refinements, to insure a high quality mesh.

FLUENT/UNS solves the RANS equations with a pressure based finite volume scheme. The SIMPLE algorithm, with second order accuracy, solves the discretized equations with multi-grid acceleration. An unstructured grid was used to allow for an accurate representation of the cooling hole without paying a significant penalty in increased numbers of cells. It is common for unstructured grids to have higher levels of numerical diffusion due to low order schemes and mis-alignment between the flow direction and the grid. To reduce the numerical diffusion, a second order accurate scheme was chosen. FLUENT/UNS is also a solution-adaptive code which can make grid refinements based on computed gradients in the flow solution. This powerful tool makes the solver better equipped for resolving regions of high gradients and complex flows. The grid refinements performed in this study also insure that the quality of the grid will be preserved because each of the marked cells are simply divided into eight new cells. The solution-adaptive refinement is also helpful for establishing grid independent results.

The FLUENT/UNS solver also offers the choice of various turbulence models, an important feature for the present study. The turbulence models tested were the standard k-ε model (Launder and Spalding, 1974) and the RNG k-ε model (Yakhot and Orszag, 1986), where RNG refers to Renormalization Group. The standard k-ε model uses a turbulent eddy viscosity to provide closure for the RANS equations and was chosen because of its success in a wide range of turbulent flow calculations. The RNG k-ε model is different from the k-ε model in that it was derived using a rigorous statistical technique (scale elimination), has an additional term in the dissipation transport equation to sensitize the solution to rapidly strained flows, and uses an analytical formula for the turbulent Prandtl number. In the literature, the RNG k-ε model is classified as a well-suited model for flows involving separation, recirculation, high curvature, and rapid strain rates. The RNG model would then be the most suited model for use in the present simulations, but the lack of application and validation of the model owed itself to a comparison.

With film-cooling simulations, not only is the turbulence model important, but also the near-wall treatment. Near-wall turbulence modeling can be divided into two different approaches: the near-wall resolution approach and the wall function approach. The near-wall resolution requires a grid resolution of $y^+ \sim 1$ to accurately resolve the full boundary layer. This resolution produces grid sizes exceedingly large for this three-dimensional problem as well as requiring long CPU times. These requirements then, in fact, no longer provide a benefit of using CFD for these three-dimensional film-cooling applications. The wall function approach allows a savings in the grid size requirements since the wall boundary cell is only required to be inside the log law region of the boundary layer. The minimum y^+ value for the wall function models is a $y^+ = 11$, with an optimal near-wall distance between $20 < y^+ < 50$. Only the wall function approach was used for this paper.

The k-ε and RNG k-ε model are both high Reynolds number models and therefore lose accuracy in the low Reynolds number, near-wall region. The wall function approach, as mentioned above, links the wall region to the fully turbulent region. Two different wall functions are offered by FLUENT/UNS: equilibrium (Launder and Spalding, 1974) and non-equilibrium (Kim and Choudhury, 1995) wall functions. The equilibrium wall functions satisfy the logarithmic law of the wall for mean velocity and temperature and assume turbulent equilibrium conditions prevail (i.e., production equals dissipation). Non-equilibrium wall functions go a step further by including the effects of pressure gradients in the law of the wall equation. Additionally, non-equilibrium wall functions compute the budget of turbulent kinetic energy (TKE) at each cell to account for the difference in the proportions of the viscous sublayer and fully turbulent layer at each cell, which is known to vary from cell to cell in non-equilibrium flows. Both wall function models were compared in this study to illustrate the improvements obtained with the non-equilibrium approach.

To insure grid independence, the same procedure that was followed for the flat plate benchmark was also used for the leading edge benchmark. That procedure included both increasing the number of cells and using adaptive procedures. The exact procedure for the leading edge computation included using a total of four different grids with each grid progressively becoming finer. There was an increase in the total number of cells for these four grids resulting in an increase of cells from 154,000 to 171,000 and an adaption for the final grid bringing it to 207,000 cells. It is more relevant, however, to compare of the number of cells inside the cooling holes and in the near-hole region (excluding the plenum and the freestream flow area). That number of cells increased from 69,500 to 92,000 (before adaption) as the grids got progressively finer. In determining whether the results were grid independent, a comparison of adiabatic effectiveness predictions were made at several streamwise positions. In comparing the last two grids, the average change in adiabatic effectiveness values across the entire computational span at x/d = 1.24 and 4.86 were $d\eta = \pm 0.007$ and ± 0.003. This grid was then adapted, based on the flow gradients, resulting in an increase from 92,000 to 120,200 cells in the cooling hole and near-hole region. The average change in adiabatic effectiveness across the entire computational span at $x/d = 1.24$ and $x/d = 4.86$ was $d\eta = \pm 0.005$ and $d\eta = \pm 0.006$. This final, adapted grid with a total number of 207,000 cells was considered to be grid independent.

The convergence criteria for these computations involved two steps. First, convergence was considered to be close when the exiting mass flowrate was within 0.01% of that entering the computational domain, which typically required around 3000 iterations for the flat plate and

1500 iterations for the leading edge benchmark. After the mass flowrate balance was close, the second step was to monitor the outflow pressure and the adiabatic effectiveness for at least 200 more iterations to insure that these values did not change.

The platform used for these computations was an IBM-SP2 parallel processor that has a total of 16 nodes. The mesh sizes created for the film-cooling benchmarks ranged from 120,000 to 220,000 cells. This required computers that offer 120M to 220M of RAM, which can only be found on advanced workstations or parallel processors. The meshes were generally split into 6 partitions and run for 30 to 40 hours to reach a converged solution.

FLAT PLATE FILM-COOLING BENCHMARK

As mentioned in the introduction, this study was a blind simulation and therefore experimental data was not available to validate the leading edge film-cooling simulation. This required us to do an in-house validation of the code for film-cooling flows where data was available in the literature. In particular, the CFD package needed to be evaluated in terms of the unstructured tetrahedral grid, turbulence models, and near-wall treatments. The flat plate film-cooling study of Sinha, et al. (1991) was chosen as a test case. Sinha, et al. measured adiabatic effectiveness values for a row of round film-cooling holes inclined in the streamwise direction at 35° for high density ratio jets. The test case chosen for the flat plate benchmark was a density ratio of DR = 2.0, because of its match to real engine conditions, and a blowing ratio of M=0.5.

Figure 1a shows the experimental set-up and the computational domain. The computational domain starts 19d in front of the trailing edge of the hole which corresponds to a sharp leading edge for their experimental test plate. A 20 m/s constant velocity was set at the inlet of the domain and an outflow boundary condition was set at the exit of the domain. An outflow boundary condition implies that the diffusion terms are set to zero. Note that the plenum, cooling hole, and the mainstream were all included in this simulation. Leylek and Zerkle (1994) were the first to point out the importance of modeling the plenum and coolant hole. The turbulent kinetic energy and dissipation rate were also set at the mainstream inlet and plenum based on isotropic assumptions, Equations (1a and 1b), where C_μ is the standard k-ε model constant $C_\mu = 0.09$, and Tu (%) is the turbulence intensity of the closed loop wind tunnel, Tu = 0.2 %. There was no attempt in modifying any of the turbulence model coefficients for either the flat plate or leading edge simulations.

$$TKE = \frac{3}{2}\left(U_\infty \cdot \frac{Tu(\%)}{100}\right)^2 \qquad \varepsilon = \frac{C_\mu^{3/4} TKE^{3/2}}{d} \qquad (1a, b)$$

The solution domain of the flat plate benchmark was discretized into 215,000 cells with an average cell skewness of 0.315. There were 18 cells across the diameter as shown in Figure 1b, giving an average wall resolution of y^+=28. The plenum had an average of y^+=10 and the test plate had an average y^+ ranging from y^+=12 near the film-cooling hole to y^+=40 at the mainstream exit.

Figures 2a and 2b compare the centerline and laterally averaged adiabatic effectiveness results for several turbulence models. Note that the streamwise distance, x/d, is measured from the trailing edge of the cooling hole and the spanwise distance is measured from the centerline of the cooling hole. These two figures allow a comparison of the near-wall treatment, using the equilibrium and non-equilibrium wall functions, as well as a comparison of the k-ε model and RNG k-ε model both using non-equilibrium wall functions.

The standard k- ε model with non-equilibrium wall functions gave the closest agreement with both the centerline and laterally averaged experimental results. The RNG k-ε model clearly overpredicted the cooling effectiveness at the hole centerline to the greatest extent, showing almost 30% higher values than the standard k-ε model. That is why investigating the laterally averaged results alone is deceiving because the RNG k-ε model shows a better agreement in the laterally averaged predictions indicating a larger amount of lateral spreading. The local lateral effectiveness values indicate, however, that the better agreement is a result of the high centerline values and not a better prediction of the lateral spreading. The turbulence fields for the different near wall models were also compared. Inside the cooling hole, it is typical to see turbulence levels around 20%, (Thole, et al., 1996). The k-ε model exhibited turbulent kinetic energy levels that agree with these measurements whereas the RNG k-ε model gave values much lower than those expected which is consistent with an overprediction of cooling effectiveness.

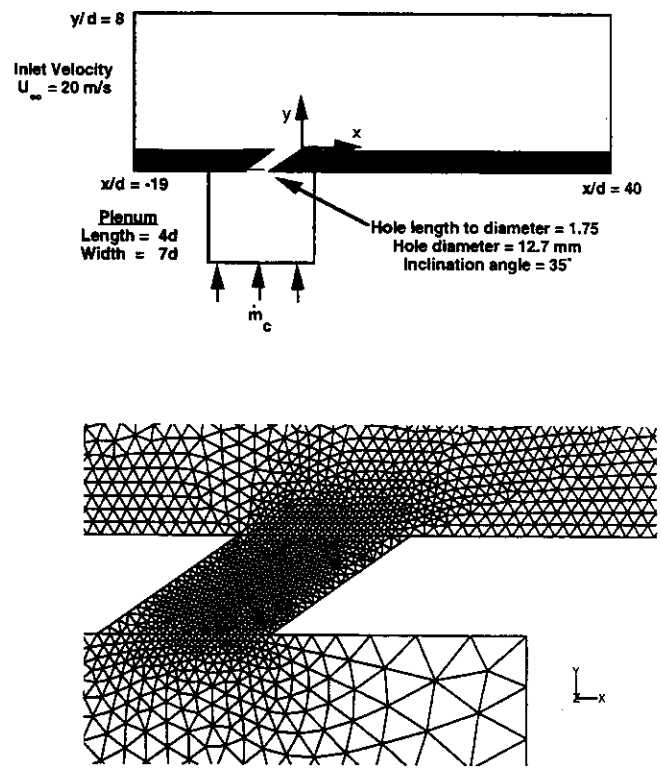

Fig. 1a,b Computational domain and close-up of the mesh for the CFD flat plate predictions and experimental results (Sinha, et al., 1991).

If the model is correct, non-equilibrium wall functions should be better at capturing the film-cooled turbulent boundary layer. In comparing the equilibrium and non-equilibrium results shown in Figures 2a and 2b, the k-ε non-equilibrium wall model does a slightly better job than the equilibrium wall model at predicting the centerline effectiveness and lateral averages. The k-ε equilibrium wall function model has a slightly higher overprediction of the centerline adiabatic effectiveness than the non-equilibrium wall model, but about the same laterally averaged effectiveness as the non-equilibrium wall model. What that means is that the prediction of the lateral spreading is much worse for the k-ε equilibrium wall model. Note that the gap between the centerline values of the equilibrium and non-equilibrium wall functions grows in the region where the jet and mainstream interaction is dominant, from the start of the jet exit to an x/d=10.

In addition to the fact that the film-cooling causes the boundary layer to be in non-equilibrium, the leading edge geometry with a highly accel-

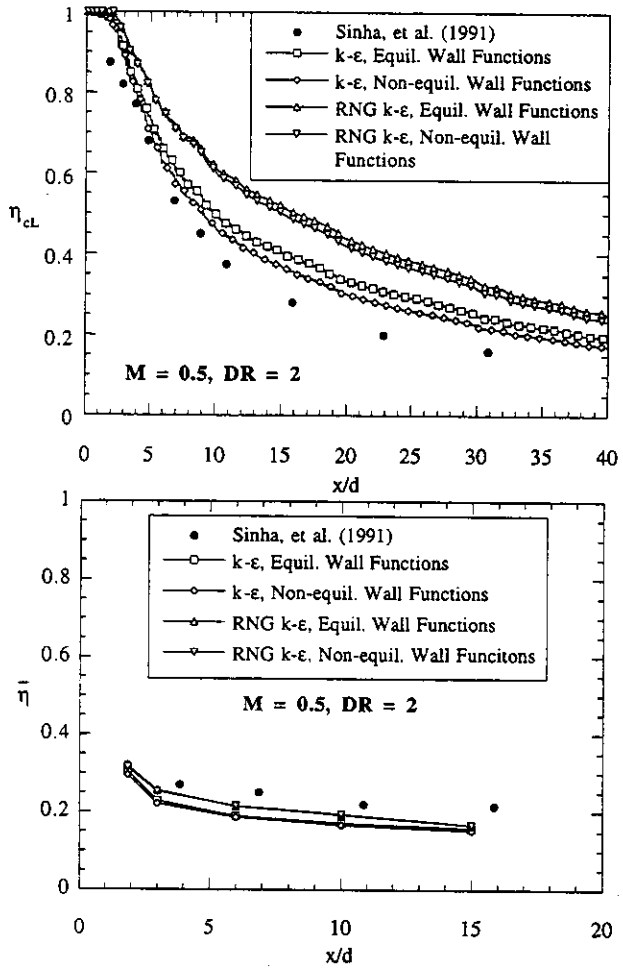

Fig. 2a and 2b Comparison of the CFD predictions and experimental results for the centerline and laterally averaged adiabatic effectiveness for the flat plate benchmark with data from Sinha, et al. (1991). Flow conditions were at ratios of M = 0.5 and DR = 2.

erating flow even worsens the possiblity for the boundary layer to be in equilibrium. The non-equilibrium model was designed by Kim and Choudhury (1995) to take into account pressure gradient effects which do occur on the leading edge geometry. In addition, this model relaxes the constraint of production = dissipation such as that assuming to occur in the equilibrium model. In conclusion, the closer match of the non-equilibrium wall function standard k-ε model to the magnitudes and trends of the experiments warranted its use for the leading edge benchmark.

LEADING EDGE COMPUTATIONAL MODEL

As discussed previously, this study was a blind CFD benchmark to compare the predicted values of adiabatic effectiveness with experimental data taken from Cruse, et al. (1997). This section describes the information provided for this study as well as the computational model that was used.

The geometry for the experimental leading edge simulation is shown in Figure 3. Two rows of staggered cooling holes, laterally spaced with a pitch of S = 7.64d, were placed at two different angular positions, θ = 0° and 25° on a quarter cylinder with a flat afterbody. Each row of cooling holes contained nine holes. The cooling hole diameters were d = 6.32 mm while the leading edge cylinder had a surface radius of R_{LE} = 50.8 mm giving a hole-to-leading edge diameter ratio of of d/D = 0.062 and a blockage ratio for the tunnel of 39%. The cooling holes themselves are injecting laterally with respect to the streamwise direction, α = 90°, and have an injection angle relative to the surface of β = 20°.

In the Cruse, et al. (1997) experimental set-up, a suction slot was just in front of the leading edge cylinder with an adjustable slot width to allow for positioning of the stagnation streamline relative to the cooling holes. For this particular benchmark study, the stagnation streamline was such that it hit the centerline of the first row of cooling holes at θ = 0°. In addition to the geometry, only the experimental conditions listed in Table 1 were given to the investigators for this CFD study.

Table 1. Experimental Conditions Given for the CFD Test Case

Freestream Velocity (m/s)	10	Mass Flow / Hole (g/s)	0.725
Freestream Turbulence (%)	0.5	$(P_{o,c}-p_\infty)$ (mm H_2O)	36.7
Freestream Temperature (C)	27.5	Plate Conductivity (W/mK)	0.025
Pressure (atm)	1	Surface Roughness (μm)	< 25
Jet/Freestream DR	1.8	Hole Edge Radius (mm)	< 0.1
Average Mass Flux Ratio	2.0	Inlet Mainstream Profile	—

The numerical domain is shown in Figure 4a. This simulation modeled the mainstream flow, the coolant supply plenum, and only one and a half cooling holes. A symmetric boundary condition about the spanwise axis for the θ = 0° cooling hole allowed simulating only half of this hole. This symmetry boundary condition matched the experimental condition of attaining a straight streamline that hit the θ = 0° hole centerline. A periodic boundary condition in the span allowed the model to have only one hole in each of the rows.

The inlet boundary condition in the mainstream was provided by Cruse, et al. (1997), and was essentially a uniform 10 m/s (within ±1%). The mainstream exit boundary condition was set to an outflow condition while the inlet boundary condition to the coolant plenum was set to a mass flowrate for one and a half holes that represented an average blowing ratio of M = 2. This mass flowrate setting assumed that equal mass flows exited both the θ = 0° and 25° cooling hole rows. This assumption was a first guess based on an inviscid analysis estimating the local static pressure at the jet exit and will be discussed further in the next section. The turbulent kinetic energy and dissipation for the plenum and mainstream were based on Equations 1a and 1b with Tu = 0.5%. The test surface was considered adiabatic with no lateral or streamwise conduction effects because of the low thermal conductivity of the Polystyrene model, was also considered to be smooth, and the cooling holes were assumed to have sharp corners.

The grid, with an average cell skewness of 0.33, contained 207,000 cells after adaption and is shown in Figure 4b. There were typically seven cells across the hole diameter giving a y^+ between $30 < y^+ < 50$ inside the cooling holes. On the external surface, the y^+ values varied, but in the near-hole region most cells had a $y^+ \sim 15$.

LEADING EDGE RESULTS

One important aspect of this problem is the prediction of the mass flux split between the two rows of cooling holes. Information given to the investigators for this blind CFD test, shown in Table 1, only indicated that the mass flowrate supplied to the cooling holes was sufficient to give an average blowing ratio of M = 2. The CFD results showed that the mass flux split between the two rows of cooling holes was very close in that 48% of the coolant exited the stagnation hole and 52% of the coolant exited the hole located at 25°. Recall, that the initial assumption was that half the massflow exited each row of holes. That assumption was needed because the CFD model only included one and a half holes

based on the periodic and symmetric boundary conditions. The resulting flow split predicted by the CFD model confirmed that the initial assumption of an approximate equal flow split was sufficient and, both rows of holes could be considered to have an average blowing ratio of M = 2. Note that the blowing ratio for both holes is defined based on the upstream mean velocity of 10 m/s. As another check to the CFD benchmark, the driving pressure difference between the coolant plenum and upstream static pressure was experimentally measured to be $(P_{o,c} - p_\infty)$ = 36.7 mm H_2O while the computed pressure difference was 36.4 mm H_2O.

In modeling only half the hole at the stagnation location (0° cooling hole), an inherent assumption was that the sharp-turning entrance effect for this hole was symmetric about the hole centerline. The hole length-to-diameter ratio for these holes is quite long at L/d = 11.75, as compared with mainbody cooling holes having relatively short hole lengths, typically between 3 < L/d < 6. This relatively long hole length can be considered to be sufficient to attain fully-developed flow as predicted by a correlation (Eqn. 12-2) given in Kays and Crawford (1993) that includes the effect of Reynolds number. Using this correlation with a jet Reynolds number of Re =1.4 x 10^4, a development length of seven hole diameters is predicted.

Figures 5a and 5b show a comparison of the normalized velocity and turbulent kinetic energy profiles as the flow develops through the cooling hole. Note that a comparison is being made between the hole located at θ = 0°, which has a symmetric boundary condition and therefore the velocity profile is only shown for the top half of the hole, with the hole located at θ = 25°, which includes the entire hole in the CFD model. At x_h/d = 3, the effect of the inlet separation can be seen on both the velocity and TKE profiles with the profiles being slightly non-symmetric. As the flow continues down the hole to x_h/d = 9, both the velocity and TKE profiles look quite symmetric for the θ = 25° hole and the agreement between the θ = 0° and θ = 25° holes looks quite good. Note that at x_h/d = 6 and 9, the mean velocity profiles look quite similar, but the TKE has decreased between x_h/d = 6 and x_h/d = 9. Based on these comparisons, the symmetric boundary condition imposed on this bottom cooling hole was acceptable for these calculations.

Figures 5c and 5d show the total velocity contours at the exit of the cooling hole for both the θ = 0° and 25° holes. These total velocities are normalized with the total jet velocity for each respective cooling hole. For the θ = 0° cooling hole, the CFD predictions show that there is a slightly larger region of low speed fluid exiting near the back edge of the cooling hole and, as expected due to the injection angle, higher speed jet fluid is exiting from the front edge (left side on Figure 5c) of the cooling hole. In contrast where there is a strong crossflow for the θ =25° cooling hole, the flow pattern is quite skewed as shown in Figure 5d. A large portion of the jet is being pushed by the mainstream toward the downstream side of the cooling hole. In addition, the coolant is primarily leaving from the back edge (left side of Figure 5d) of the cooling hole. This skewing causes much higher velocities to be exiting from that portion of the cooling hole.

The following sections discuss the surface adiabatic effectiveness predictions followed by a discussion of the flow and thermal field predictions. In particular, this section addresses a comparison of the CFD predictions with those experimentally measured values of adiabatic effectiveness and thermal fields presented by Cruse, et al., (1997). Note that the coordinate system for these results are such that the normalized dis-

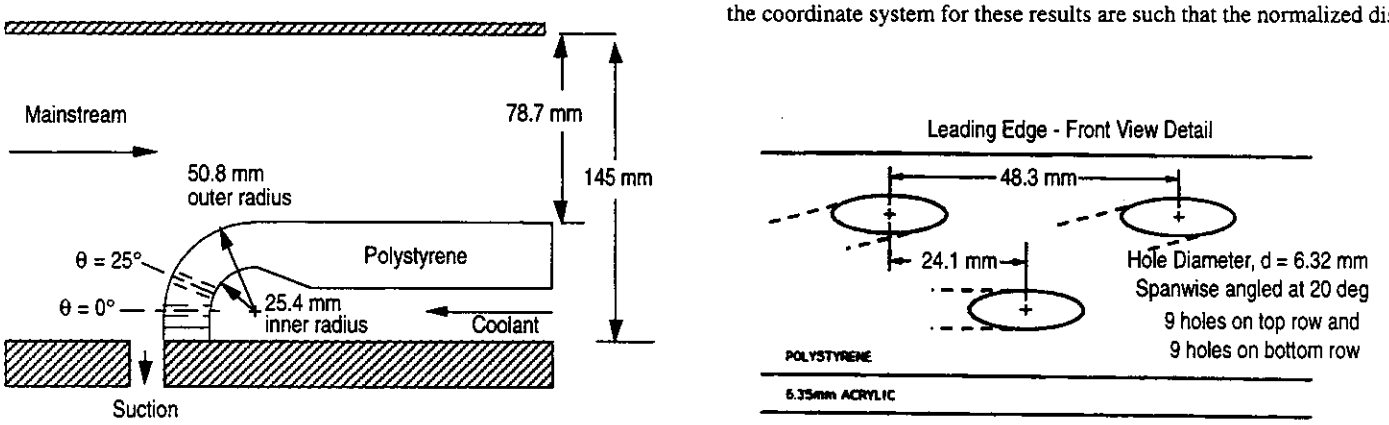

Fig. 3 Experimental facility by Cruse, et al. (1997) used for the leading edge benchmark (left) and the leading edge front view (right).

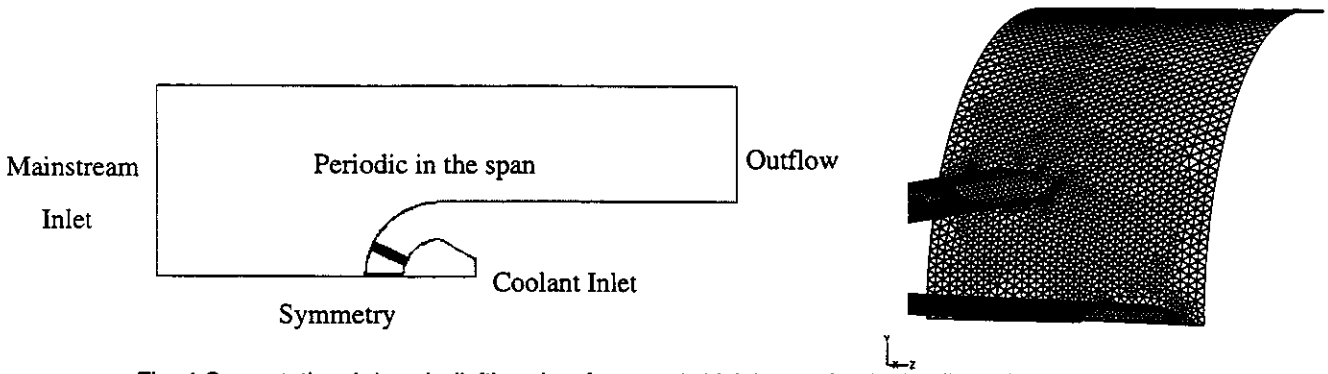

Fig. 4 Computational domain (left) and surface mesh (right) used for the leading edge simulation.

tance along the surface in streamwise direction, denoted by x/d, has an origin located at the centerline of the 0° stagnation hole and the normalized lateral distance, denoted by z/d, has an origin located at the edge of the 25° hole. The direction normal to the leading edge surface is noted as y/d.

Surface Adiabatic Effectiveness Predictions

Figures 6a and 6b show surface adiabatic effectiveness contour results measured with those predicted through CFD, respectively. The general trends of the CFD predictions agree with those measured. The cooling jets at the stagnation location (x/d = 0) do a relatively good job in terms of spreading the coolant laterally to cover a large surface area. In contrast, the second jet is swept downstream with relatively little lateral coverage. Note that the average blowing ratio is M = 2 for both the 0° and 25° holes, as discussed previously, where this blowing ratio is based on the far upstream velocity (U_∞ = 10 m/s). The local crossflow velocity, however, for the two hole locations is quite different in that for the stagnation hole the local crossflow velocity is zero and for the 25° hole the local crossflow velocity is 8.45 m/s giving a local blowing ratio for the 25° hole of M = 2.36. The streamwise sweep for the θ = 25° coolant hole is because of the strong crossflow that is present relative to the no crossflow for the stagnation hole at θ = 0°.

Figure 7a shows the comparison between predicted and measured lateral distributions of adiabatic effectiveness at x/d = 1.24 (just downstream of the θ = 0° cooling hole), x/d = 4.86 (just downstream of the θ = 25° cooling hole) and x/d = 9.98.

The non-equilibrium wall function approach that was used in this benchmark study, was able to do a relatively good job in predicting the spread of the coolant as compared to the experimentally measured. At the x/d = 1.24 location, the coolant distribution as measured through the experiments is uniformly spread whereas the CFD predictions show a much more 'sinusoidal' shape with definite peaks and valleys. This is, in fact, due to a slight cooling jet separation at the leading edge which was not predicted through CFD. These results are consistent with flat plate film-cooling results in that using CFD with the same turbulence models there is an overprediction in the laterally averaged adiabatic effectiveness at a high blowing ratio in which jet detachment has been shown to occur experimentally.

Moving further downstream on the leading edge at x/d = 4.86, the width of the jets for both the experiments and CFD agree fairly well while the primary differences being that the CFD overpredicts the peak values and there is only a slight shift in the exact spanwise location of that peak value. At x/d = 4.86, a peak value at approximately z/d = 3 was predicted by CFD of η = 0.95 relative to the experiments having a peak level of η = 0.7. The difference between the experiments and the CFD predictions for the tails (at z/d > 4) at x/d = 4.86 is a result of what is leftover from missing the prediction of the first row jet separating. Similarly at x/d = 9.98, the width of the jet is still predicted quite well with the difference being in the peak values and a slight shift of that peak value. At an x/d = 9.98, the peak level for the CFD results was η = 0.6 whereas the measurements gave a level of η = 0.4.

Figure 7b shows the laterally averaged adiabatic effectiveness values. In general, there is good agreement between CFD and measured values for the laterally averaged effectiveness except near the stagnation location and immediately downstream of the θ = 25° hole with CFD overpredicting at both locations. Turbine designers using state-of-the art CFD codes to design cooling holes can interpret these results by noting that the predicted laterally averaged values are fairly accurate. If, however, a flow feature such as a jet detachment/reattachment occurs, these current CFD models may not be suitable for that prediction.

Flow and Thermal Fields

Figures 8a and 8b give a comparison between the CFD predicted and experimentally measured non-dimensional thermal field profiles at x/d = 1.24, 4.86 and 9.98. Note that the non-dimensional temperature corresponds to the same normalization used for the surface temperature in the adiabatic effectiveness, i.e., Θ = 1 represents the jet temperature and Θ =

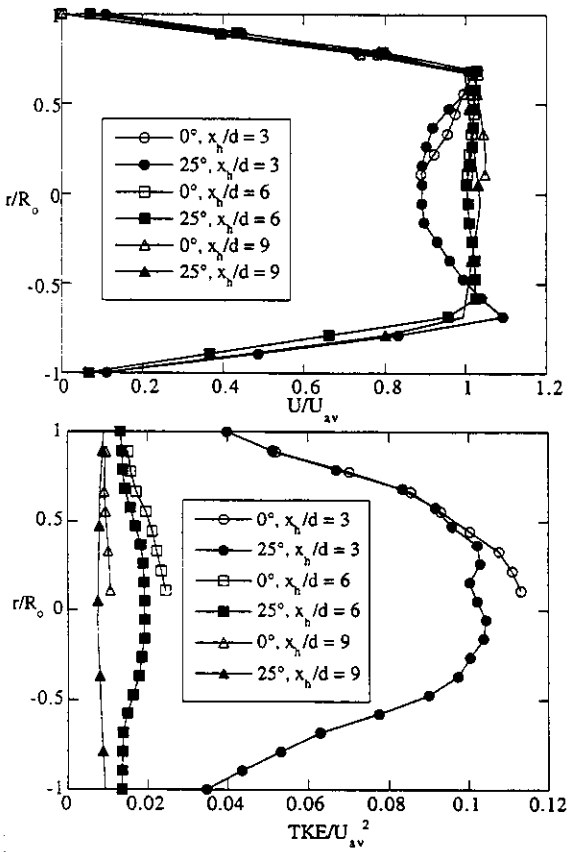

Fig. 5a,b Axial mean velocity and TKE profiles inside the leading edge film-cooling holes for the θ = 0° and 25° holes.

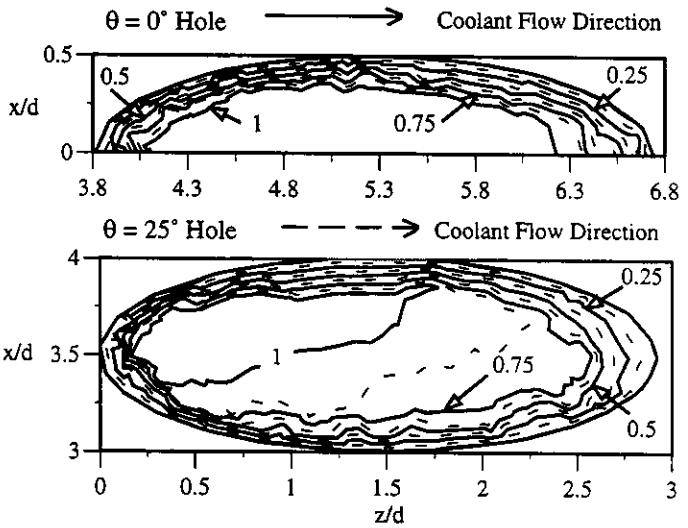

Fig. 5c,d Total velocity contours for the θ = 0° (top) and 25° (bottom) leading edge film-cooling holes.

0 represents the freestream temperature. Also note that under the thermal field contour plots the solid lines and the dashed lines show the locations for the θ = 0° and 25° holes, respectively.

As with the surface adiabatic effectiveness plots, the largest differences between the CFD and experimental results is the point closest to the stagnation region at x/d = 1.24. In addition to predicting a colder peak jet temperature, the CFD results indicate that the coldest part of the jet is centered around z/d = 2 while the experimental results show the peak is at the start of the coolant hole at z/d = 4. This cold region for the experiments being so far away from the hole is a remnant of the separated fluid at the stagnation point, which was not predicted by the CFD analysis. Further downstream, the agreement between the CFD and experimental thermal fields are much better as was also indicated by the laterally averaged effectiveness. The overall width, height, and contour levels of the jet at both x/d = 4.86 and 9.98 are in good agreement.

The adiabatic effectiveness contours of Figure 6 for both the measured and CFD results show that there is a relatively large spanwise region in which cooling takes place all the way from the stagnation cooling hole at θ = 0° to the start of the second cooling hole at 25°. In fact, the CFD predictions show that the jet pathlines, shown in Figure 9, indicate that coolant fluid leaving the θ = 0° cooling hole passes directly over the cooling hole located at θ = 25°. Figure 9 shows a front view of the leading edge pathlines as the fluid exits the θ = 0° and 25° holes while the gray scale of the pathlines is in terms of the same normalized temperature as the thermal fields. Note that as the coolant fluid from the θ = 0° hole passes over the cooling hole at θ = 25° the two fluids mix cooling the jet fluid from the θ = 0° hole. This results in a poor use of the coolant fluid from the θ = 0° cooling hole as also confirmed by Salcudean, et al. (1994) who observed the same effect for two rows of staggered holes.

Again in Figure 8 downstream of the θ = 25° cooling hole at x/d = 4.86, the thermal fields are somewhat skewed with steeper temperature gradients at z/d = 4, which is a spanwise location farthest from the jet exit. The severe crossflow of the mainstream is preventing the coolant from penetrating into the lateral direction causing steep temperature gradients on the side of the jet farthest from the hole exit. On the other side of the jet at z/d = 1.75 there is a curling of the jet inwards causing the contours to appear skewed. This inward motion is clearly seen on Figure 9 which shows the jet fluid pathlines. As the jet exits the left side of the cooling hole, this relatively low-speed jet fluid is pulled inward and under the jet fluid that exits from the center of the coolant hole.

Figure 10 shows the normalized turbulent kinetic energy contours for the same locations as the thermal fields. At x/d = 1.24, the peak turbulent kinetic energy contour coincides with the top jet/mainstream interface. At x/d = 4.86, the peak turbulent kinetic energy contour coincides

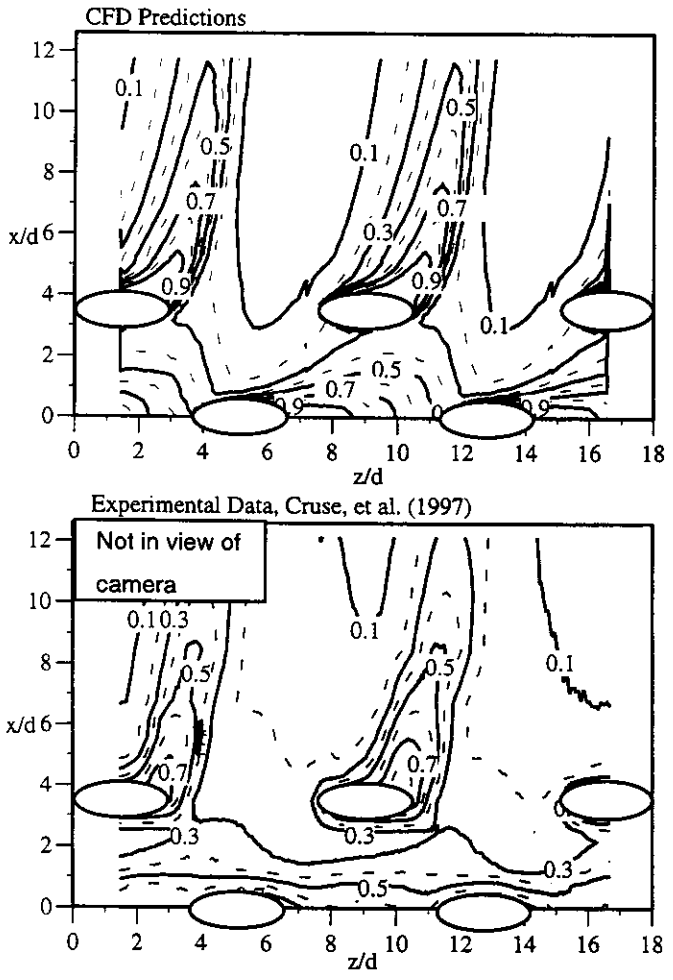

Figs. 6a,b Comparison of adiabatic effectiveness contours, mapped along the leading edge surface, predicted using CFD (top) and experimentally measured (bottom) for a DR = 1.8 and M = 2.

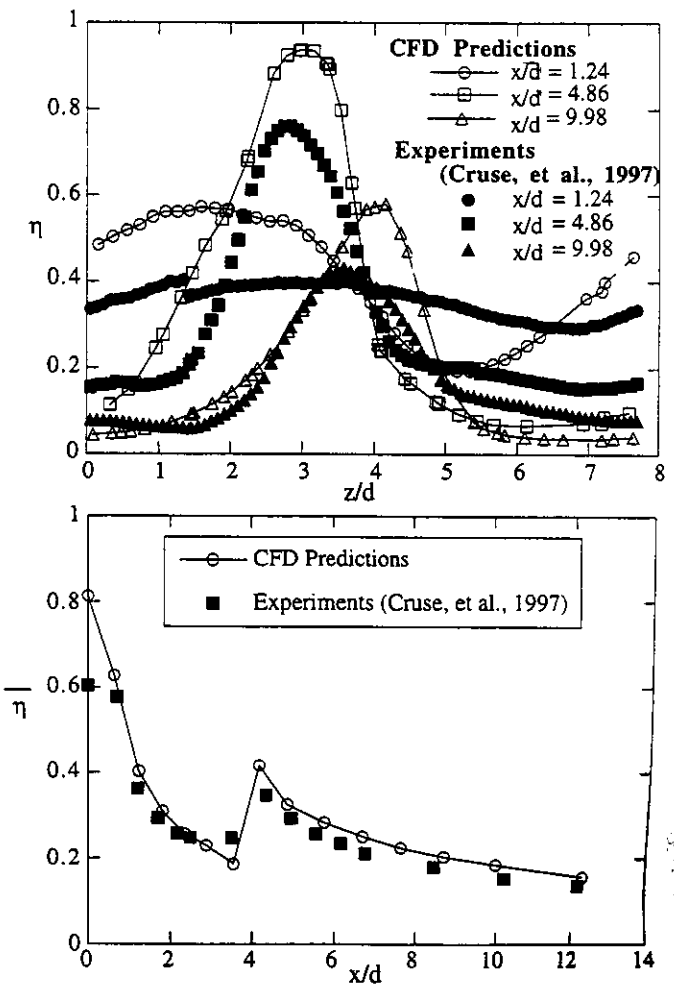

Figs. 7a,b Comparison of measured and CFD predicted local (top) and laterally averaged (bottom) adiabatic effectiveness contours for DR = 1.8 and M = 2.

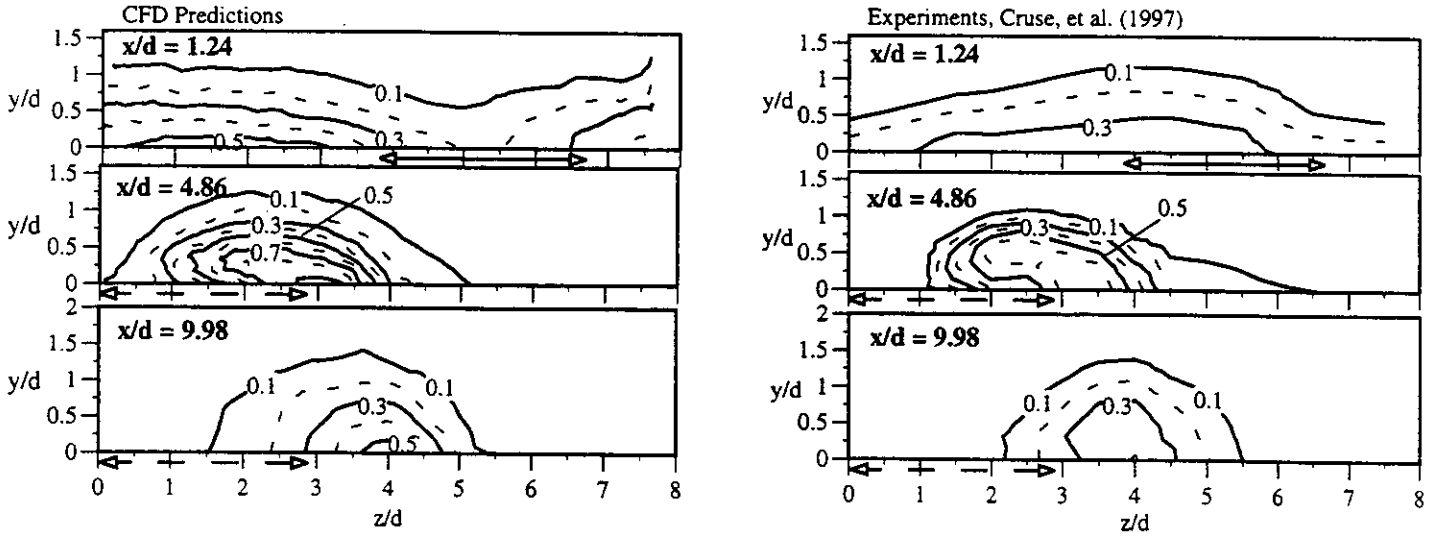

Fig. 8 Comparison of thermal field contours predicted through CFD (left) and experimentally measured by Cruse, et al. (1997) (right).

with the top left side of the jet/mainstream interface and corresponds to the side of the jet closest to the jet exit. Recall that the skewed thermal field contours showed a more diffuse jet on the left side of the jet which is due to this highly turbulent region.

CONCLUSIONS

A benchmark against published data for a flat plate film-cooling flowfield and a blind benchmark for a leading edge film-cooling flowfield showed that it is feasible to use CFD as a design tool to get a reasonable estimate of the cooling characteristics. The flat plate simulation showed that using a k-ε model with non-equilibrium wall functions gave the best agreement to the experimental results as compared with some of the other models that are available.

The results indicated that using a CFD model for the leading edge geometry consisting of a spanwise periodic boundary condition and a symmetry boundary condition at the stagnation location allowed an adequate representation of the flowfield. The major discrepancy between the CFD predictions and the experimental results for the leading edge geometry was at the stagnation location in which there was a small separation region that was not predicted using CFD. Although the peak levels of adiabatic effectiveness were overpredicted using CFD, the laterally averaged adiabatic effectiveness values agreed quite well with the experimental results.

The adiabatic effectiveness contours showed that the lateral spreading was quite good for the $\theta = 0°$ stagnation cooling hole, but that some of the cooling fluid was interacting with the $\theta = 25°$ coolant fluid rather than being used to cool the surface. Relative to the $\theta = 0°$ cooling jet, the $\theta = 25°$ cooling jet did not laterally spread very successfully resulting in very low adiabatic effectiveness values between the cooling holes. The high crossflow at the exit for the $\theta = 25°$ cooling hole, relative to the $\theta = 0°$ cooling hole, resulted in the jet quickly being swept downstream.

Jet pathlines showed that some of the fluid leaving the $\theta = 0°$ cooling hole interacts with the left side of the $\theta = 25°$ cooling hole. Note that the

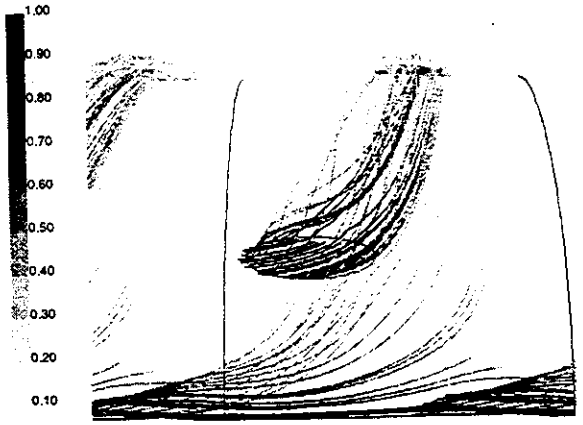

Fig. 9 Coolant flow pathlines exiting the leading edge holes.

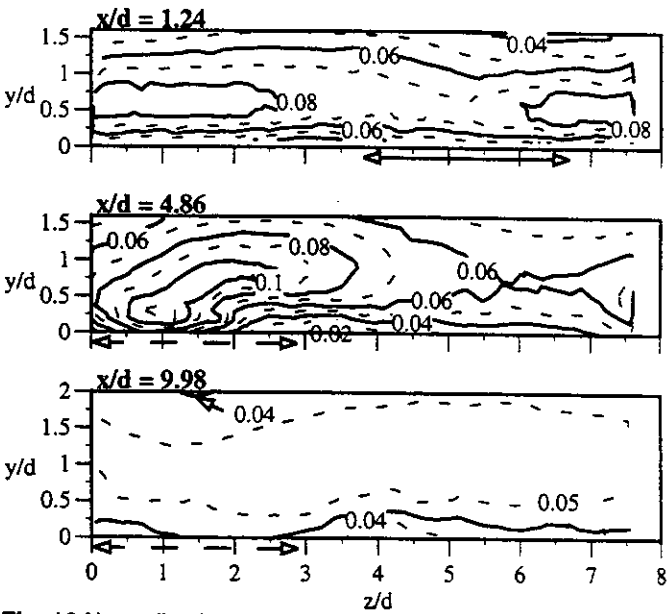

Fig. 10 Normalized turbulent kinetic energy (TKE/U_∞^2) contours for the leading edge film-cooling case at a DR = 1.8 and M = 2.

jets were blowing from left to right in these calculations. This $\theta = 0°$ fluid is initially cooled when passing over the second hole, but then very quickly heats up again and is mixed with the fluid leaving the second cooling hole at $\theta = 25°$. This left side of the jet shows a spread in the thermal contours and corresponds to very high turbulent kinetic energy levels that extend from the top edge of the jet all the way down to the surface.

The final conclusion is that CFD is a valuable tool, as shown by this blind benchmark study, to help give a good understanding to a very complicated flowfield where field measurements are quite difficult and time intensive. This CFD study has also shown that laterally averaged adiabatic effectiveness predictions can be used with confidence.

ACKNOWLEDGEMENTS

The authors sincerely thank Martin Tabbita, Dean Johnson, and Fred Soechting in the Turbine Components Center of Pratt & Whitney, Florida for their support.

REFERENCES

Benz, E. Wittig, S., Beeck, A., and Fottner, L. (1993) "Analysis of Cooling Jets near the Leading Edge of Turbine Blades," presented at the 72nd Fluid Dynamics panel meeting and symposium on Computaional and Experimental Assessment of Jets in Cross Flow, Winchester, U.K. AGARD-CP-534, Paper No. 37.

Cruse, M. W., Yuki, U. M., and Bogard, D. G. (1997) "Investigation of Various Parametric Influences on Leading Edge Film Cooling," submitted to the International Gas Turbine and Aeroengine Congress and Exposition, Orlando, Florida.

FLUENT/UNS User's Guide (1996)Release 4.0, Fluent, Inc., N. H.

He, P, Salcudean, M. and Gartshore, I. (1995) "Computations of Film Cooling for the Leading Edge Region of a Turbine Blade Model," presented at the International Gas Turbine and Aeroengine Congress and Exposition, Houston, Texas, ASME paper no. 95-GT-20.

He, P., Licu, D., Salcudean, M. and Gartshore, I. (1996) "Leading Edge Film Cooling: Computations and Experiments Including Density Effects," presented at the International Gas Turbine and Aeroengine Congress and Exposition, Birmingham, UK, ASME paper no. 96-GT-176.

Karni, J. and Goldstein, R. J. (1990) "Surface Injection Effect on Mass Transfer From a Cylinder in Crossflow: A Simulation of Film Cooling in the Leading Edge Region of a Turbine Blade," *ASME Journal of Turbomachinery*, vol. 112, pp. 418-427.

Kays, W. M. and Crawford, M. E. (1993) Convective Heat and Mass Transfer, 3rd Edition (McGraw-Hill: New York).

Kim, S. and Choudhury, D. (1995) "A Near-Wall Treatment Using Wall Functions Sensitized to Pressure Gradient," ASME Fluids Engineering Div. Summer Conference, August, 1995, Hilton Head, SC.

Launder, B. E. and Spalding, D. B. (1974) "The Numerical Computation of Turbulent Flows," *Computer Methods in Applied Mechanics and Engineering*, vol. 3, pp. 269-289.

Leylek, J. H. and Zerkle, R. D.(1994) "Discrete-Jet Film Cooling: A Comparison of Computational Results with Experiments," *ASME J. of Turbomachinery*, vol. 113, pp. 358-368.

Mayle, R. E. and Anderson, A. (1991) "Velocity and Temperature Profiles for Stagnation Film Cooling," *ASME J. of Turbomachinery*, vol. 113, pp. 457-462.

Mehendale, A. B. and Han, J. C. (1992a) "Influence of High Mainstream Turbulence on Leading Edge Film Cooling Heat Transfer," *ASME J. of Turbomachinery*, vol. 114, pp. 707-715.

Mehendale, A. B. and Han, J. C. (1992b) "Influence of High Mainstream Turbulence on Leading Edge Film Cooling Heat Transfer: Effect of Film Hole Spacing," *International Journal of Heat and Mass Transfer*, vol. 35, no. 10, pp. 2593-2604.

Mehendale, A. B. and Han, J. C. (1993) "Reynolds Number Effect on Leading Edge Film Effectiveness and Heat Transfer Coefficient," *International Journal of Heat and Mass Transfer*, vol. 36, no. 5, pp. 3723-3730.

Mick, W. J. and Mayle, R. E. (1988) "Stagnation Film Cooling and Heat Transfer, Including Its Effect within the Hole Pattern," *ASME J. of Turbomachinery*, vol. 110, pp. 66-72.

Ou, S., Mehendale, A. B., and Han, J. C. (1992) "Influence of High Mainstream Turbulence on Leading Edge Film Cooling Heat Transfer: Effect on Film Hole Row Location," *ASME J. of Turbomachinery*, vol. 114, pp. 716-723.

Ou, S. and Han, J. C. (1992) "Influence of Mainstream Turbulence on Leading Edge Film Cooling Heat Transfer through Two Rows of Inclined Film Slots," *ASME J. of Turbomachinery*, vol. 114, pp. 724-733.

Ou, S. and Han. J. C. (1994) "Leading Edge Film Cooling Heat Transfer through One Row of Inclined Film Slots and Holes Including Mainstream Turbulence Effects," *ASME J. of Heat Transfer*, vol. 116, pp. 561-569.

Salcudean, M. Gartshore, I., Zhang, K. and Barnea, Y. (1994) "Leading Edge Film Cooling of a Turbine Blade Model through Single and Double Row Injection: Effects of Coolant Density," presented at the International Gas Turbine and Aeroengine Congress and Exposition, The Netherlands, ASME paper no. 94-GT-2.

Sinha, A. K., Bogard, D. G., and Crawford, M. E. (1991) "Film Cooling Effectiveness Downstream of a Single Row of Holes with Variable Density Ratio," *ASME J. of Turbomachinery*, vol. 113, pp. 442-449.

Thole, K. A., Gritsch, M., Schulz, A., and Wittig, A. (1997) "Effect of a Crossflow at the Entrance to a Film-Cooling Hole," to appear in the *ASME J. of Fluids Engineering*, September.

Walters, D. K. and Leylek, J. H. (1996) "A Systematic Computational Methodology Applied to a Three-Dimensional Film-Cooling Flowfield," presented at the International Gas Turbine and Aeroengine Congress and Exposition, Birmingham, UK, ASME paper no. 96-GT-351.

Yakhot, V. and Orszag, S. A. (1986) "Renormalization Group Analysis of Turbulence: I. Basic Theory," *Journal of Scientific Computing*, vol. 1, pp. 1-51.

Zhou, J., Salcudean, M., and Gartshore, I. (1993) "Prediction of Film Cooling by Discrete-Hole Injection," presented at the International Gas Turbine and Aeroengine Congress and Exposition, Cincinnati, Ohio, ASME paper no. 93-GT-75.